2017 2nd International Conference on Architectural Engineering and New Materials (ICAENM 2017)
ISBN: 978-1-60595-436-3

Cavitation Simulation of Highly Skewed Propellers

Jian Hu, Qingyuan Huang, Ting Guo, Chong Geng and Shili Sun

ABSTRACT

Blade skew plays an important role in the prohibition of propeller cavitation and needs to be analyzed quantitatively. For this purpose, the cavitation of model propellers with different skew DTMB4381, 4382, 4383 and 4384 are investigated using commercially available software Ansys-Fluent. The $k-\omega$ SST model was used for turbulence modeling, and the QUICK scheme was selected as the discretization scheme. The results show that present simulation is accurate and reliable for predicting the propeller hydrodynamics with cavitation. On this basis, the influences of different skew on the appearance of cavitation are analyzed. It is found that the highly skewed blade can effectively delay the occurrence of cavitation.[1]

INTRODUCTION

It is well known that the cavitation can exacerbate noise radiation, vibration transmission and efficiency reduction, which will eventually deteriorate the function of marine crafts. One of the alternatives to prohibit the cavitation is the application of highly skewed propeller, whose major feature is that the blade edge has a sweep angle along the direction of rotation, so that each radius section of the blade does not enter the high wake. For these reasons, it is of great interest and significance to investigate the cavitation of a skewed propeller.

At present, there are two major methods used in the numerical simulation of propeller cavitation. One is the boundary element method based on the potential flow assumption. A low-order potential-based 3-D BEM was used to model the flow around 3-D partially cavitating hydrofoils [1], and 3-D cavitating

[1]Jian Hu, Qingyuan Huang, Ting Guo, Chong Geng, Shili Sun*, College of Shipbuilding Engineering, Harbin Engineering University, Harbin, Heilongjiang, China

propellers [2]. The BEM method is effective in the simulation of partial or super cavitation, but the method fails to simulate the flow separation and can only be applied in the simulation of sheet cavitation. Then, recent research was turned to RANSE simulation, in which Navier-Stokes equation is solved numerically.

Comparing with potential based method, RANSE simulation is more physical and has the potential in successful simulation of bubble cavitation and vortex cavitation. Thus, the latter method is used to perform the numerical simulation of the cavitation. Firstly, convergence study is conducted and the results are verified by experimental data. Then, extensive simulation is performed to investigate the effect of skew on propeller cavitation.

METHODOLOGY AND NUMERICAL MODELS

Governing Equation

The Reynolds averaging approach for turbulence modeling is applied, the Navier-Stokes equations [3] can be written in Cartesian form as

$$\frac{\partial(\rho_m)}{\partial t}+\frac{\partial(\rho_m u_i)}{\partial x_i}=0. \qquad (1)$$

$$\frac{\partial(\rho_m u_i)}{\partial t}+\frac{\partial(\rho_m u_i u_j)}{\partial x_j}=-\frac{\partial p}{\partial x_i}+\frac{\partial}{\partial x_j}\left[\mu(\frac{\partial u_i}{\partial x_j}+\frac{\partial u_j}{\partial x_i}-\frac{2}{3}\delta_{ij}\frac{\partial u_l}{\partial x_l})\right]+\frac{\partial}{\partial x_j}(-\rho u_i' u_j') \qquad (2)$$

.

where δ_{ij} is the Kronecker delta, and $-\rho u_i' u_j'$ the Reynolds stresses. These Reynolds stresses must be modeled to enclose Eq. 2. It is usually necessary to introduce the Boussinesq assumption that the Reynolds stress is proportional to the mean velocity gradient. That is

$$-\rho u_i' u_j' = u_t\left(\frac{\partial u_i}{\partial x_j}+\frac{\partial u_j}{\partial x_i}\right)-\frac{2}{3}(\rho k+u_t\frac{\partial u_i}{\partial x_i})\delta_{ij}. \qquad (3)$$

Turbulence Model

The two-equation model of RANS is applied. This model was proposed by Menter [4] in 1994, which solved the problem of over-dependence of free flow in previous models. The equations can be described as

$$\frac{\partial(\rho k)}{\partial t}+\frac{\partial(\rho u_j k)}{\partial x_j}=\frac{\partial}{\partial x_j}\left[\left(\mu+\sigma_k\mu_t\right)\frac{\partial k}{\partial x_j}\right]+\tau_{ij}\frac{\partial \mu_i}{\partial x_j}-\beta^*\rho\omega k. \qquad (4)$$

$$\frac{\partial(\rho\omega)}{\partial t}+\frac{\partial(\rho u_j\omega)}{\partial x_j}=\frac{\partial}{\partial x_j}\left[\left(\mu+\sigma_\omega\mu_t\right)\frac{\partial\omega}{\partial x_j}\right]+\frac{\gamma}{\nu_t}\tau_{ij}\frac{\partial\mu_i}{\partial x_j}-\beta\rho\omega^2+2\left(1-F_1\right)\rho\sigma_{\omega^2}\frac{1}{\omega}\frac{\partial k}{\partial x_j}\frac{\partial\omega}{\partial x_j}\quad .\quad (5)$$

Cavitation Model

Numerical simulation of cavitation is based on solving transport equations coupled with the mass and momentum conservation equation. Taking into account the fluid density ρ_m as a function of vapor mass fraction f [5]. The $\rho_m - f$ relationship is

$$\frac{1}{\rho_m}=\frac{f}{\rho_v}+\frac{1-f}{\rho_l}. \quad (6)$$

where ρ_v is the vapor phase density and ρ_l is the liquid phase density. The vapor mass fraction, f , is governed by a transport equation

$$\frac{\partial(\rho_m f)}{\partial t}+\nabla\cdot(\rho_m\vec{V}f)=\nabla(\Gamma\nabla f)+R_e-R_c. \quad (7)$$

where R_e is the vapor generation rate and R_c is the condensation rate. They are both functions of fluid properties and flow field parameters. R_e and R_c can be obtained by the empirical formula given by Singhal [5].

Grid Generation and Numerical Setups

Table 1 shows the principal particulars of the four model propellers. It can be seen that the other parameters of the four DTMB model propellers are basically same except the skew angle.

To ensure the numerical accuracy and efficiency, fully structured hexahedral grids are generated by using ICEM CFD (The Integrated Computer Engineering and Manufacturing code for Computational Fluid Dynamics). The computational domain consists of the rotating domain containing the propeller and the left stationary domain. Fig. 1 shows the overall layout of the flow field. The inflow and outflow boundaries are located at x=−2D and x=4D respectively. The diameter of the stationary cylindrical domain is 3D and that of the rotating domain is 1.2D. The blades were simply mounted on an infinitely long cylinder, which serves as the hub [6]. Fig. 2 shows the computational mesh on blade surface of DTMB 4384. The height of the cell adjacent to the blade surface is kept at unity in the viscous unit. Other meshing parameters are chosen following the previous studies [7, 8], so that the grid dependency is sufficiently small for the purpose of the simulation.

TABLE 1. PRINCIPAL PARTICULARS OF THE MODEL PROPELLERS.

DTMB	4383	4384
Propeller diameter[m]	0.305	0.305
Blade number	5	5
Area ratio	0.725	0.725
Pitch ratio	1.2	1.2
Skew[°]	72	108

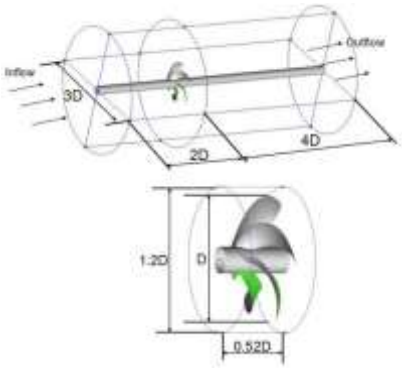

Figure 1. Layout of the flow field.

Figure 2. Blade mesh of DTMB 4384.

The commercially available software Ansys-Fluent is used as the solver, which has been successfully applied to simulate the viscous flow around marine propellers. The $k-\omega$ SST model was used for turbulence modeling, and the QUICK scheme was selected as the discretization scheme. The pressure-velocity coupling is treated SIMPLEC algorithm, and the second-order upwind scheme is adopted for pressure, density and momentum.

Verification of Numerical Results

To verify the reliability of the present numerical models and the meshing strategy, convergence study is performed and the numerical results are verified by the experimental data in this section. For convenience, the non-dimensional thrust coefficient K_T, torque coefficient K_Q, advance coefficient J, and cavitation number σ are defined as following

$$K_T = \frac{T}{\rho n^2 D^4}. \tag{9}$$

$$K_Q = \frac{Q}{\rho n^2 D^5} . \tag{10}$$

$$J = \frac{V_0}{nD} . \tag{11}$$

$$\sigma = \frac{p_0 - p_v}{\frac{1}{2}\rho V_0^{\,2}} . \tag{12}$$

where T is the propeller thrust, Q is the propeller torque, ρ is the water density, n is the rotation rate, D is the propeller diameter, V_0 is the uniform flow velocity; p_0 is the reference pressure, and p_v is the vapor pressure.

For details, propeller rotation speed is 600 rpm, the advance coefficient is 0.7, and the flow velocity can be calculated according to Eq. (11). The saturated vapor pressure of the water is 2350 Pa, corresponding to 20 ℃. The non-condensable gas mass fraction is set to 1.26e-7. The pressure control factor, density control factor, volume force control factor, momentum control factor, turbulence kinetic energy control factor, dissipation rate control factor and the turbulence viscosity control factor is all modified to 0.2.

Convergence study was performed with respect to DTMB4381 which has no skew and the results are shown in Fig. 3. It can be seen the present fairly good converged results can be obtained as the grid number is smaller as 50 million by the fully structured meshing strategy in Fig. 2. For better grid independency, in the following simulation, the grid number is 250 million if not specified.

Fig. 4 presents the comparison of the non-cavitating hydrodynamic loads. It can be seen that the numerical results are slightly larger than those by experiments [9]. As the advance velocity coefficient decreases, the numerical results gradually deviate from the numerical data. But in overall, fairly accurate K_T and K_Q can be obtained by present numerical scheme.

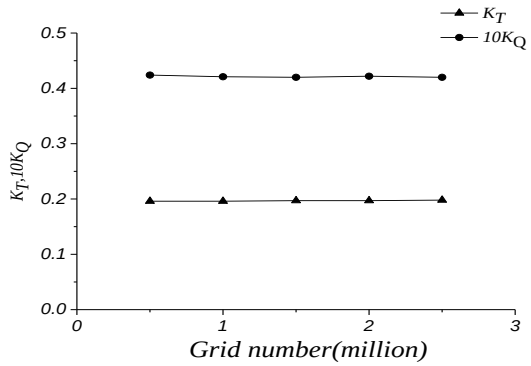

Figure 3. Convergence study with respect to grid number.

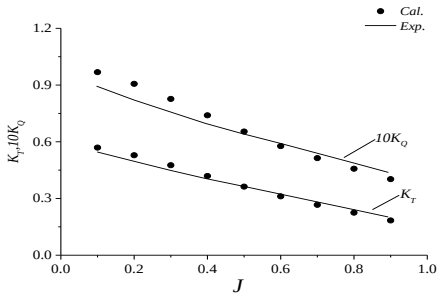

Figure 4. Comparison of K_T and K_Q for non-cavitating DTMB4381.

Fig. 5 presents the comparison of K_T and K_Q for cavitating DTMB4384 as $\sigma = 2.0$. The numerical accuracy can also be verified. Moreover, Fig. 5 shows the significant effect of cavitation on the K_T and K_Q. Comparing the value with the non cavitating results in Fig. 4, it is found K_T and K_Q drop by 19.1% and 7.3%, respectively. Fig. 6 shows the comparison of the cavitation appearance of numerical and experimental results as $\sigma = 3.5$ and $J = 0.7$, and they agree with each other very well.

Generally, the numerical results by the present meshing strategy and the numerical models have good agreement with those by experiments, which validates the reliability of the present numerical simulation.

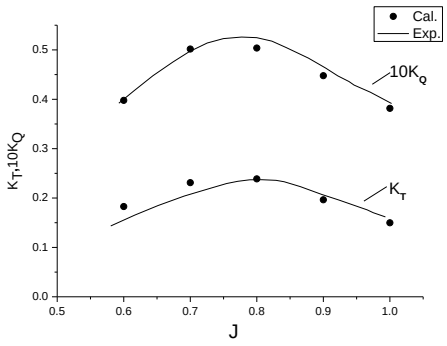

Figure 5. Comparison of K_T and K_Q for cavitation DTMB4384. ($\sigma = 2.0$ and $J = 0.7$).

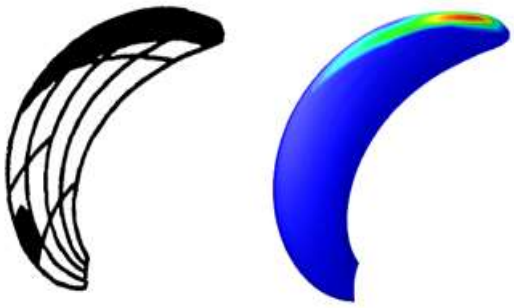

(a) Experimental result (b) Numerical result

Figure 6. Comparison of the cavitation appearance ($\sigma = 3.5$ and $J = 0.7$).

Discussions

Fig.7 shows the numerical cavitation of DTMB4383 and DTMB4384 as $\sigma = 3.0$ and $J = 0.7$.

Listed in Table 1, the skew angles of DTMB 4383 and 4384 are 72° and 108°, respectively. It can be seen through the comparison that the cavitating region is very different. With the increase of the skew angle, the cavitation is significantly prohibited. At the same operating condition, the cavitation of DTMB4381 starts from 0.4R to tip, while that of DTMB 4384 starts from 0.6R, and the cavitating area is much smaller. This indicates the higher skew of the blade can effectively prohibit the cavitation of a propeller.

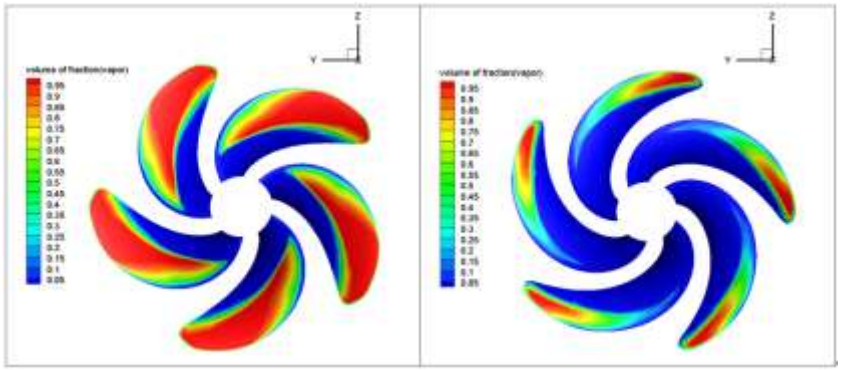

(a) 4383 propeller (b) 4384 propeller

Figure 7. Cavitating appearance of DTMB 4384 and 4384, $\sigma = 3.0$ and $J = 0.7$.

CONCLUSIONS

In this paper, the cavitation performance of a highly skewed propeller DTMB4384 is investigated through RANSE simulation. The numerical simulation is verified by the experimental data. The result shows that RANSE is suitable for predicting the cavitation performance of skewed propellers. It is found the skew is effective in the prohibition of propeller cavitation.

ACKNOWLEDGEMENTS

The authors are grateful for the support of the National Natural Science Foundation of China (Grant Nos. 51678045, 51579052).

REFERENCES

1. Fine N E, Kinnas S A. A boundary element method for the analysis of the flow around 3-D cavitating hydrofoils [J]. Journal of Ship Research, 1993, 37(3): 213-224.
2. Kinnas, S., Fine, N., 1992. A nonlinear boundary element method for the analysis of unsteady propeller sheet cavitation. In: Nineteenth Symposium on Naval Hydrodynamics, Seoul, Korea, pp. 717-737.
3. Seo J H, Seol D M, Lee J H, et al. Flexible CFD meshing strategy for prediction of ship resistance and propulsion performance[J]. International Journal of Naval Architecture and Ocean Engineering, 2010, 2(3): 139-145.
4. Menter F R. Two-equation eddy-viscosity turbulence models for engineering applications[J]. AIAA Journal, 1994, 32(8): 1598-1605.
5. Singhal A K, Athavale M, Li H, et al. Mathematical basis and validation of the full cavitation model [J]. Journal of Fluids Engineering, 2002, 124(3): 617-624.
6. Rhee S H, Joshi S. Computational validation for flow around a marine propeller using unstructured mesh based Navier-Stokes solver [J]. JSME International Journal Series B, 2005, 48(3): 562-570.
7. Kawamura T, Omori T (2009) Reynolds number effect on propeller performance in open water. J Jpn Soc Nav Archit Ocean Eng 10:29-36.

8. Kawamura T (2011) Numerical simulation of propulsion and cavitation performance of marine propellers. J JIME 46(3):3590365.
9. Boswell R J. Design, cavitation performance, and open-water performance of a series of research skewed propellers[R]. David W Taylor Naval Ship Research And Development Center Bethesda Md, 1971.